Journal of Power Sources 196 (2011) 9188–9194

Contents lists available at ScienceDirect

Journal of Power Sources

journal homepage: www.elsevier.com/locate/jpowsour

Degradation of the Pt/C air cathode in acidic solution examined by cyclic thermammetry

G. Smith, G.T. Burstein*

Department of Materials Science and Metallurgy, University of Cambridge, Pembroke Street, Cambridge, CB2 3QZ, United Kingdom

ARTICLE INFO

Article history:
Received 28 April 2011
Received in revised form 28 June 2011
Accepted 5 July 2011
Available online 12 July 2011

Keywords:
Air cathode
PEM fuel cell
Degradation
Platinum
Cyclic thermammetry

ABSTRACT

The oxygen reduction reaction on carbon-supported platinum electrocatalysts (Pt/C) has been investigated as a function of temperature by employing the technique of cyclic thermammetry. A novel electrochemical cell has been designed which allows the concomitant measurement of the potentiostatic current from the oxygen reduction reaction (ORR) and accurate control of the aqueous electrolyte temperature, allowing cyclic linear temperature sweeps between 25 and 80 °C at speeds up to 40 mK s^{-1}. Our method provides new insight into the temperature dependent degradation of the cathodic oxygen reduction reaction in aqueous sulfuric acid systems. Cycling the temperature accelerates the degradation of the cathodic current through loss of active surface area. Two simultaneously operating mechanisms are proposed to account for this loss. One mechanism is described by physical detachment of the platinum and carbon particles under thermal fatigue, and the other by anodic dissolution of the Pt electrocatalyst. The forms of these are discussed.

1. Introduction

The proton exchange membrane fuel cell (PEMFC) is one of the promising technologies for clean power generation in transport and portable applications [1–3]. However, a well-known issue preventing the practical implementation of these systems is the degradation of the cathode electrocatalyst [4], typically nanoparticulate Pt supported on high-surface-area carbon. The loss of electrocatalytically active surface area (EAS) is known to be a major factor in contributing to the decay in performance [5,6]. Of the major mechanisms that may account for EAS loss, the most common are: (a) dissolution/redeposition of Pt causing particle growth [7], (b) dissolution and migration of mobile Pt^{2+} [8], or (c) corrosion of the carbon support onto which the platinum is dispersed [9].

In the recent literature the performance degradation of the PEMFC is generally studied *ex situ* by postmortem microscopy and by *in-situ* cyclic voltammetry [10–12], techniques which attempt to recreate the exposure of the cathode to the high potentials that occur during start-up and shut-down procedures in an operating PEMFC. In addition to the well-researched overpotential fluctuations on the cathode within this system, it is also evident that during such procedures and within an operating fuel cell, temperature variations are likely to be present [13,14]. The effect of temperature on the kinetics of the ORR has been researched [15–18], but very little has been done to determine the effect of temperature on the degradation of the PEMFC [19]. In addition, the current literature uses constant temperature conditions, which are easy to maintain experimentally, but which may fail to simulate the continual temperature variations that would be present in an operating PEMFC.

It is the purpose of the present study to design a system capable of implementing the technique of cyclic thermammetry to enable such a characterisation. The technique allows measurement of electrochemical parameters as continuous functions of an imposed cyclic temperature ramp [20–24]. We simulate the expected cathode environment in the PEMFC by using a conventional aqueous three-electrode electrochemical cell modified to accommodate measurement by cyclic thermammetry. This work reveals a significant degradation rate, accelerated by cycling the temperature, which we are able to observe as it occurs, and which is dependent upon the applied oxygen reduction overpotential.

2. Experimental

A novel aqueous three-electrode electrochemical cell using a Hg/Hg_2SO_4/saturated K_2SO_4 reference electrode (MMS) was employed. The reference electrode was housed in a side-arm remote from the main cell to maintain a reference electrode temperature of 23 °C irrespective of the temperature of the working cell. All potentials quoted in this work have been converted to the standard hydrogen electrode (SHE) scale. The potential of the working electrode (WE) was controlled by a Solartron 1286

* Corresponding author. Tel.: +44 1223 334361; fax: +44 1223 334567.
E-mail address: gtb1000@cam.ac.uk (G.T. Burstein).

0378-7753/$ – see front matter © 2011 Elsevier B.V. All rights reserved.
doi:10.1016/j.jpowsour.2011.07.011

electrochemical interface. Both the cathode and anode were of diameter 20 mm, comprising 0.4 mg Pt cm^{-2} gas diffusion electrodes (GDEs) stamped out from a parent sheet supplied by Johnson Matthey. All experiments were carried out using deaerated analytical grade H_2SO_4 (3 mol dm^{-3}, 0.1 dm^3) prepared using twice-distilled water. Determination of the true surface area was performed using high purity BIP grade argon from Air Products and 10% CO in N_2 from BOC gases. Air "Zero" (a simulated air composition of 20.9% O_2, 79.1% N_2), and hydrogen "Premier Plus" gas (Air products) were used as the feed cathode and anode gases respectively for electrochemical measurements under cyclic thermammmetry. To test the effect of the nitrogen component in air, "Premier" grade oxygen (99.995%) from Air Products was used as an alternative feed cathode gas. Air, oxygen and hydrogen were all maintained at a constant flow rate of 28 cm^3 (at STP) min^{-1}, which was sufficient to ensure a large excess stoichiometry of oxygen (in air) at the maximum current density reported here.

These experiments are designed to allow the programmed variation of temperature at constant potential (cyclic thermammetry) [20–24] or programmed variation of potential at constant temperature (cyclic voltammetry). For this, a new electrochemical cell was designed and built, as shown in Fig. 1. This design allowed cyclic thermammetry to be used as a fuel-cell technique by providing accurate programmed control of the electrolyte temperature through both heating and cooling cycles. The electrochemical cell is equipped with ports, labeled 1–3 in Fig. 1. The functions of the ports are as follows:

1. Ports labeled 1 allow linear cooling to be achieved by assisted cold-water cooling via an external pump. The speed of the peristaltic pump is regulated by an amplifier which detects the difference between the programmed and true electrolyte temperatures.
2. Ports labeled 2 allow sensing and control of the internal and external jacket temperatures by glass-encapsulated thermistors.
3. Ports labeled 3 allow connection of a nitrogen-fed gas-lift pump to deoxygenate the aqueous electrolyte. This also functions as a convector to circulate the heat supplied by a coil of nickel-chromium wire threaded around the exterior of the Pyrex-glass gas-lift pump (not shown). The power supplied to the heater was also regulated by a feedback control unit designed and built in-house.

This system provided both precise control of the electrolyte temperature and quantitative measurement of the electrochemical thermal response of the ORR between 25 and 80 °C, scanned linearly and cyclically at a rate up to 40 mK s^{-1}.

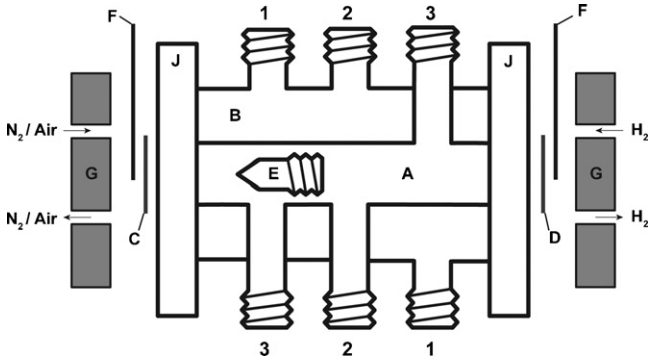

Fig. 1. Schematic drawing of the glass electrochemical cell showing the double-jacketed electrolyte compartment. (A) Internal compartment filled with electrolyte, (B) external water filled compartment, (C) cathode (working electrode), (D) anode (counter electrode), (E) Luggin capillary port for reference electrode, (F) gold foil current collector, (G) Perspex cell housing, (J) glass flanges to enable sealing of the cell housing.

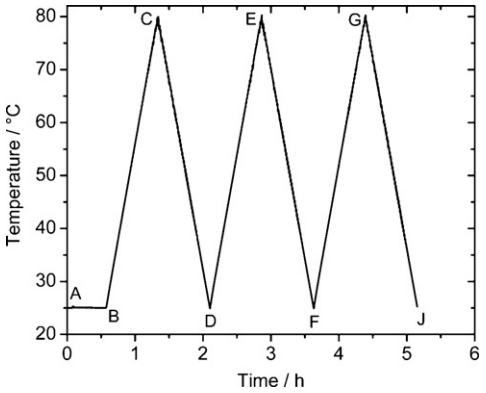

Fig. 2. A typical temperature profile used for cyclic thermammetry tests. A–B: 30 min dwell at 25 °C to ensure ORR is at steady state before thermammetry, B–J: Continuous heating and cooling between 25 and 80 °C at constant sweep rate.

2.1. Surface area determination

The true surface areas of the working electrode before and after thermammetric treatment were determined by carbon monoxide stripping voltammetry, using a method similar to that published previously [25]. These CO-stripping experiments were performed at a constant temperature of 25 ± 0.1 °C. While maintaining the counter electrode under argon, the working electrode was initially polarised potentiostatically at 0.15 V(SHE) under argon, before changing the inlet gas to 10% CO in N_2. The adsorption of CO was monitored under potentiostatic control for 2 min. This period was sufficient to ensure complete adsorption of carbon monoxide. After adsorption, the WE gas feed lines were purged with argon for 10 min to eliminate any free CO as well as that reversibly adsorbed on the electrode surface. The WE was then polarized potentiodynamically for 12 cycles between 0.05 and 1.2 V(SHE) at 10 mV s^{-1} under argon flow, which ensured that any remaining traces of adsorbed CO had been removed.

2.2. Cyclic thermammetry

After initial surface area measurement, the feed gases to the WE and CE were changed to air (or pure oxygen) and pure H_2 respectively, and the system was allowed to re-equilibrate at open circuit. For the thermammetry measurements, a constant potential, cathodic relative to the ORR equilibrium potential, was then applied while the electrolyte temperature was swept according to a predefined programme. All temperature sweeps used for the present experiments were linear with time, and both heating and cooling ramps employed the same temperature sweep-rate magnitude. A typical temperature profile is shown in Fig. 2.

After the temperature sweeps had been terminated, the gases to both electrodes were changed back to argon and the cell allowed to equilibrate at 25 °C before a final surface area measurement was performed. Some cyclic thermammetry experiments were also carried out using electrodes that had not been exposed to carbon monoxide, to ensure that there was no residual effect of prior exposure to CO, and to check the reproducibility.

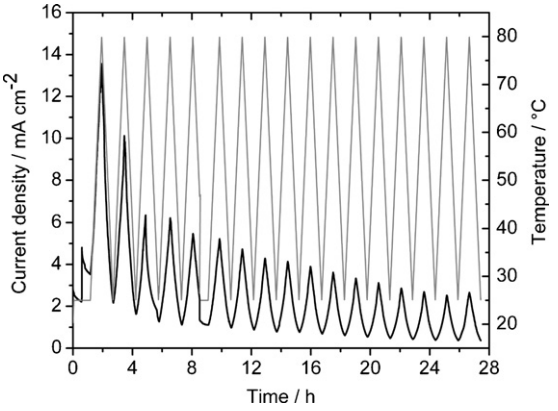

Fig. 3. Cathodic current density response to a linear temperature sweep between 25 and 80 °C at 20 mK s^{-1} over 17 cycles for the ORR at 0.8 V(SHE). Cathodic current density shown in black, temperature program in grey.

3. Results

3.1. Degradation of the cathode at high potential

Fig. 3 shows a typical response of the cathodic current from the Pt/C WE as a result of the thermal cycling under potentiostatic polarisation at 0.8 V(SHE). The figure shows 17 successive cycles. Each thermal cycle shows that the cathodic oxygen reduction current increases with temperature during the heating stage, and decreases during the cooling stage, as is expected from the Arrhenius relationship. Fig. 3 also shows there is a significant reduction in the cathodic current density with increasing cycle number: each successive cycle lies at a smaller cathodic current density than the previous cycle for a given temperature. This degradation in the performance of the cathode occurs over successive temperature cycles, resulting in the peak current density (measured at the highest temperature of 80 °C) falling from 13.6 to 2.6 mA cm^{-2}, a decrease of 81%, over the 17 cycles (*ca.* 28 h) of the experiment.

We illustrate the degradation in performance of the cathode by using the current density maximum in each temperature cycle, measured at the highest temperature of 80 °C. These data are plotted in Fig. 4(a) and (b). Fig. 4(a) illustrates the dependence on time of the cathodic current density at 80 °C and 0.9 V(SHE) for different temperature sweep rates. One set of data measured at the lower potential of 0.8 V(SHE) is also plotted. The current density in each case was normalised to the 80 °C peak value from the first temperature cycle: the data represent essentially the decay of performance relative to the first cycle. We point out the following features. First, the rate of degradation in performance is fastest at the beginning for each graph, and slows down with time. Second, the decay of cathodic current density with time is faster for higher temperature-sweep rates: it is clear that the degradation rate of the electrode is a function of the temperature sweep rate. Third, when comparing the data measured at the two electrode potentials, it is observed that the decay in performance is initially independent of the potential: the data for the first 2 cycles are the same for both potentials. However, as further temperature cycling is imposed, it is also apparent that the rate of degradation is slower at 0.8 V(SHE) than it is at the higher potential of 0.9 V(SHE).

Fig. 4(b) shows the same data plotted as a function of the cycle number, rather than time. This graph shows that at 0.9 V(SHE) the percentage decay in performance with respect to the number of temperature cycles is the same (within the scatter), independent of the temperature sweep rate. This illustrates that the degradation kinetics are approximately independent of time itself, but depend primarily on the number of thermal cycles. The data representing 0.8 V(SHE) show trends similar to those of Fig. 4(a): initially the degradation rate is the same as that at the higher potential, but then becomes relatively slower.

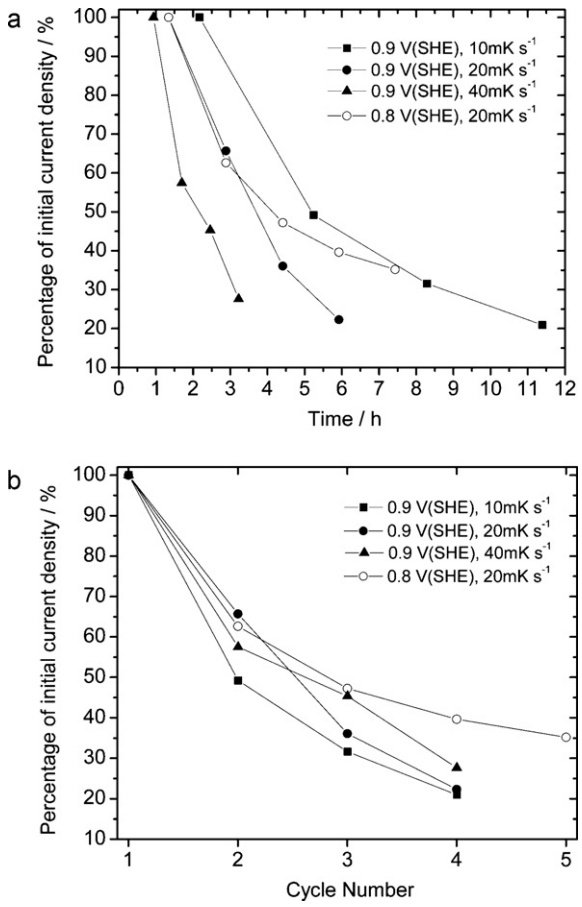

Fig. 4. Figures show the degradation in cathodic current density at 80 °C for 10, 20 and 40 mK s^{-1} at 0.9 V(SHE) (black data points) and for 20 mK s^{-1} at 0.8 V(SHE) (white data points). Data are normalised to the 80 °C value of the first temperature cycle. The first cycle then represents 100% activity. (a) Percentage of initial cathodic current density against time. (b) Percentage of initial cathodic current density against cycle number.

3.2. Degradation of the cathode at low potential

The response of the cathodic current from the Pt/C WE was also examined at the much lower electrode potential of 0.3 V(SHE), and this is shown in Fig. 5. Two experiments were carried out here,

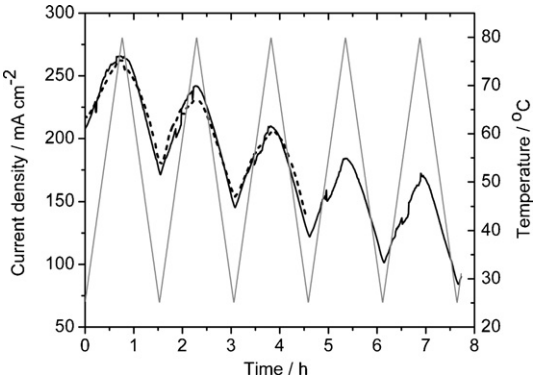

Fig. 5. Current density response to a linear temperature sweep between 25 and 80 °C at 20 mK s^{-1} for two identical electrodes at 0.3 V(SHE). Cathodic current density shown in black (shown dashed for 3 cycles, sample 1a and solid for 5 cycles, sample 1b). Temperature program in grey.

on two identical electrodes stamped from the same parent sheet, to demonstrate the typical high degree of reproducibility achieved during cyclic thermammetry testing. One was carried out over 5 thermal cycles and the other over only 3 cycles: the experiments were otherwise identical. The reproducibility is very high, with a maximum error of ~3% between the peak current densities for the different samples of the same catalyst. The degradation in performance of the cathode is still pronounced, despite the much lower potential used here. In addition, the degradation in current density continues to occur at the same rate for cycles 4 and 5. It is noteworthy, however, that the degree of degradation at 0.3 V(SHE) over the 5 cycles (35.8% from Fig. 5) is much lower than the degree of degradation observed at 0.8 V(SHE) over the same time period (60% from Figs. 3 and 4(a)).

Anodic CO stripping voltammetry was carried out in order to quantify the loss of electrochemically active surface area (EAS) due to degradation at 0.3 V(SHE). Fig. 6 shows the CO stripping cyclic voltammograms for both samples before and after the 3- and 5-cycle thermammetry experiments shown in Fig. 5 at this potential. As the initial EAS voltammograms (before the thermammetric measurements) were found to be identical for the two samples, only one is shown in Fig. 6. A sharp anodic peak is observed at 0.77 V(SHE) in the voltammogram due to the electro-oxidation of CO. The area under this peak was found by integration and converted to a true surface area of the electrocatalyst, in units of cm^2 of true surface area per cm^2 of projected surface area ($cm^2\,cm^{-2}$), otherwise known as the roughness factor R_f. Also calculated was the specific electrocatalytic surface area (SECSA), in units of m^2 of true surface area per gram of platinum ($m^2\,g^{-1}$). In order to convert the integrated charge into surface area, as commonly used, a charge density of 484 μC per true cm^2 was taken for the charge density required to oxidise a monolayer of CO on Pt (1 1 1) [26]. The limits for integration were defined as being the deviation from the double layer charging current on the lower potential side of the CO peak and the midpoint potential between the CO and PtO peaks on the higher potential side. Each voltammogram in Fig. 6 is labeled with the corresponding R_f and SECSA value calculated by this method.

It is apparent that the surface area of the oxygen reduction electrode, potentiostatically polarised at a potential of 0.3 V(SHE), decreases as a result of continuously cycling the temperature during thermammetry. Furthermore, the reduction in surface area is a function of the number of thermal cycles and is in good agreement with that found according to the percentage degradation in performance, as measured by the decrease in cathodic current density. This comparison is shown in Table 1. It is immediately apparent that the degradation in performance of the air cathode under temperature cycling is a direct consequence of a loss of surface area of the electrocatalyst on the cathode.

Table 1
Correlation between the percentage reduction in current density due to temperature cycling at 0.3 V(SHE) for 3 and 5 thermal cycles, and the corresponding loss of surface area measured by CO stripping voltammetry. Sample identification is as shown in Figs. 5 and 6.

Sample	No. of temperature cycles	Degradation in current density (%)	Degradation in surface area (%)
Pt/C 1a	3	21.5	22.3
Pt/C 1b	5	35.8	39

3.3. Comparison with degradation of the cathode at constant temperature

The role of thermal cycling on the degradation kinetics is now further demonstrated by comparison of the data measured under cyclic temperature sweeps with cathode performance data obtained at a constant temperature of 80 °C. This temperature is the highest used in the cyclic thermammetry experiments. Fig. 7 shows data from both constant temperature (80 °C) and cyclic thermammetry testing for two oxygen reduction potentials of 0.15 V(SHE) and 0.8 V(SHE). The low degree of degradation of the 80 °C constant temperature data at 0.15 V(SHE) (12% over 9 h) is clear. Data for the thermally cycled electrode at the same potential show a far greater rate of degradation in catalytic activity. We observe extensive degradation when the temperature is cycled at 0.15 V(SHE), giving a 33% loss in performance over the same time period (9 h) and Fig. 7 shows that the current continues to degrade at least until the end of the test. Comparison of the data from these two experiments shows the major influence that cycling the temperature has on the degradation of these systems: even at this low potential, degradation of the cathode performance occurs, and is enhanced by thermal cycling.

Fig. 7 further highlights that the decrease in cathodic current density depends not only on thermal cycling but also on the oxygen reduction potential. As before, the more significant loss is observed at the higher electrode potential of 0.8 V(SHE) (lower oxygen reduction overpotential). A fairly similar rate of degradation is observed at this potential for both constant temperature and thermamme-

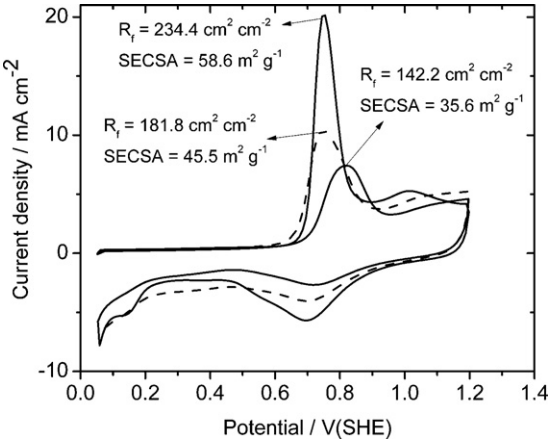

Fig. 6. CO stripping voltammograms for the as-received electrode (shown in grey) and both post-test WEs from the cyclic thermammetry treatment presented in Fig. 5 (shown dashed for 3 cycles, sample 1a and solid for 5 cycles, sample 1b). The reduction in true surface area as a result of cycling the temperature at 0.3 V(SHE) is clear. Each voltammogram is labeled with the R_f ($cm^2\,cm^{-2}$) and SECSA value ($m^2\,g^{-1}$ Pt).

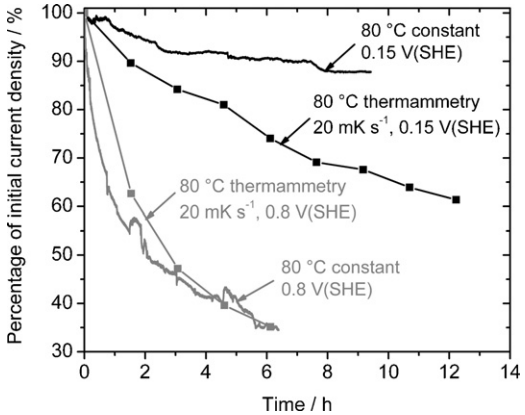

Fig. 7. Comparison of the degradation of the cathode current density between constant temperature (continuous lines) and cyclic thermammetry (with data points) experiments at 80 °C for 0.15 and 0.8 (SHE) In each case the current density has been normalised to the initial current density. The cyclic thermammetry data were obtained during temperature sweeping between 25 and 80 °C at a sweep rate of 20 mK s^{-1}.

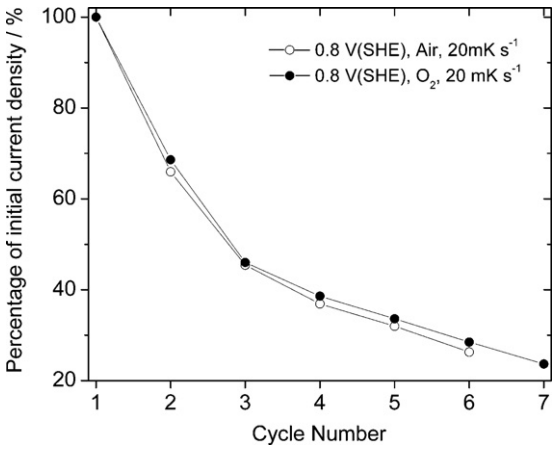

Fig. 8. The degradation in cathodic current density at 80 °C under air (open circles) and pure oxygen (filled circles) at 0.8 V(SHE) as a result of cyclic thermammetry between 25–80 °C at 20 mK s^{-1}. Data are normalised to the 80 °C value of the first temperature cycle as 100% activity.

try conditions, although this is largely fortuitous since varying the temperature sweep rate for these experiments alters the rate of degradation with respect to time, as shown in Fig. 4(a).

Finally, we present the normalised 80 °C peak data against cycle number at 0.8 V(SHE) measured under cyclic thermammetry between 25 and 80 °C at 20 mK s^{-1} under pure oxygen. These data are shown in Fig. 8, together with the corresponding information for air under otherwise identical conditions. A quantitatively similar decay in performance is observed under pure oxygen for any given thermal cycle compared with that under air. Thus, by changing the inlet gas from air to pure oxygen, no change in the high potential thermammetric degradation characteristics is observed: there is no effect from nitrogen on the degradation induced by temperature cycling.

4. Discussion

Although it is well known that Pt is not immune from corrosion within an acidic environment under potential cycling conditions [27], it has generally been found both in solution chemistry [28] and from theory [29,30] that the most extensive cathode performance losses occur at potentials above 0.8 V(SHE) because of the anodic dissolution of platinum from the electrode according to the reaction:

$$Pt \rightarrow Pt^{2+} + 2e^{-} \quad (1)$$

It is clear that for high surface area nanoparticulate systems at a potential of 0.8 V(SHE) and higher, anodic dissolution of Pt occurs and under continuous potentiostatic polarisation must account for a significant fraction of the degradation observed in Figs. 3 and 4. The role of anodic dissolution of platinum for this system is demonstrated by the fact that the degradation of the cathode is faster at 0.9 V(SHE) than it is at 0.8 V(SHE), as shown by the 20 mK s^{-1} data in Figs. 4 and 7: this is fully consistent with the expected potential dependence of reaction (1). The dissolution mechanism is expected to be effectively irreversible in the aqueous electrolyte because the dissolved Pt^{2+} would diffuse away from the WE into the bulk electrolyte, and the dissolution rate should increase as a function of temperature.

Although it has been shown to account for a high proportion of the degradation at 0.9 V(SHE), the data of Figs. 4(a) and (b) are not expected if the degradation mechanism is solely due to the anodic dissolution of platinum. If anodic dissolution were the only mechanism to cause degradation of the cathode, the slowest sweep (10 mK s^{-1}) data, having spent longer in the high temperature region, would be expected to show the fastest rate of decay in performance (with respect to time) because this experiment involved the longest time at the highest temperature. By contrast, Fig. 4(a) demonstrates that the fastest sweep rate shows the fastest rate of decay in cathode performance. In fact Fig. 4(a) shows that the rate of decay of cathode performance at constant potential increases with increase in temperature sweep rate, contrary to what is expected from anodic dissolution alone. Thus, although anodic dissolution of Pt must occur at these high electrode potentials, there must also be a second mechanism of degradation operating simultaneously as a result of thermal cycling.

The existence of a second, simultaneously operating mechanism of degradation is also evident from the experiments conducted at the low potentials (0.3 V(SHE) in Fig. 5 and 0.15 V(SHE) in Fig. 7). These are low potentials and are far below the potential at which Pt is expected to oxidize, both in the bulk form [31], and well as in nanoparticulate form [32], and so no anodic dissolution is expected to occur. However, both Figs. 5 and 7 show that the performance degrades continuously under temperature cycling. In addition, Figs. 3 and 5 were measured under identical temperature programmes, differing only in potential (0.3 and 0.8 V(SHE) respectively). The lower rate of degradation in Fig. 5 must be due to the absence of the anodic dissolution. There is nevertheless, clearly a degradation mechanism in operation at the lower potential, and this is evident by the good agreement between the degradation in cathodic current density and surface area loss shown in Table 1.

Finally, we offer convincing evidence of a second mechanism of degradation in Fig. 7, where the cathodic current density measured at the still lower potential of 0.15 V(SHE) shows degradation under temperature cycling, at a far greater rate than is observed at the maximum constant temperature of 80 °C. Again, if this were due only to anodic dissolution of Pt, or indeed any electrochemical reaction, the rate should be much higher at the constant high temperature, contrary to Fig. 7.

These facts show consistently that there is necessarily a second mechanism of degradation operating, and that this second mechanism has two immediately obvious characteristics: the second mechanism is operative at all potentials (and therefore cannot be anodic dissolution), and it is stimulated by temperature cycling, rather than by the temperature *per se*. Because of these facts, and because the effect causes a loss of surface area (Table 1), we deduce that the degradation of the cathode results from physical detachment of platinum from the carbon support particles. This occurs because of the continuous temperature cycling to which the cathode is subject during cyclic thermammetry. Such temperature cycling causes thermal stress to be generated between the platinum and carbon particles: essentially the degradation is due to a type of "thermal fatigue". In this context, thermal fatigue means damage to the Pt/C interface that is induced by continuous temperature cycling over very few thermal cycles. Indeed, much of the degradation is observed already on the first cooling and subsequent heating ramps, representing only one thermal cycle. The thermal stress at the carbon/platinum interface could be caused by the different thermal expansion coefficients for the platinum and the carbon support particles. To our knowledge, these thermal expansion coefficients for nanoparticles are unknown. However, for bulk platinum and graphite (perpendicular direction) the thermal expansion coefficients are given as 8.8×10^{-6} K^{-1} and 0.5×10^{-6} K^{-1} respectively at 25 °C [33]. These properties of bulk materials are alone sufficient to realise that differential expansion and contraction would be involved in the Pt/C system through temperature cycling. The numerical difference in expansion for the bulk materials is clearly small over the 55 K range studied: nevertheless, it is possible that nanoparticulate systems have a bigger difference in coefficient of expansion and contraction between the platinum and carbon par-

ticles, resulting in greater thermal fatigue. It is also known that unusual properties exist for nanoparticulate systems, which are different from bulk properties [32,34–36], and so it is possible that greater thermal stresses are present in these electrodes than the bulk values may suggest. Indeed, the interface between the platinum and carbon particles is not currently understood at all, and neither is the dimension of the ligament bonding them. It is therefore proposed that the nanometre scale platinum particles (diameter *ca.* 2–3 nm) expand and contract at a rate different from the more bulk-like carbon support particles (diameter *ca.* 20 nm) as the temperature is cycled. As the temperature is cycled, this continuous expansion and contraction induces a thermal fatigue between the two dissimilar particles. This causes the physical and electrical disconnection from the working electrode resulting in the reduction in surface area, and in electrocatalytic activity observed. As the rate of temperature cycling increases the thermal fatigue process is accelerated, resulting in the increased rate of degradation with respect to time entirely consistent with the data plotted in Fig. 4(a) and (b).

The data of Fig. 7 give further evidence of two simultaneous degradation mechanisms. In the absence of anodic dissolution, the data at 0.15 V(SHE) demonstrate the major influence that cycling the temperature has in the degradation of these systems. At this low potential, the degradation mechanism of nanoparticulate Pt/C is greatly accelerated by cycling the temperature at modest sweep rates. Despite the constant-temperature electrode experiencing a far longer time at the maximum temperature than the electrode subject to thermal cycling, the loss of performance at constant temperature is far lower. This again precludes anodic dissolution as the degradation mechanism at this low potential and provides further evidence of particle detachment as a result of thermal fatigue. Fig. 7 also illustrates the contribution of anodic dissolution to degradation at the higher potential by the similarity in degradation rate between constant temperature and thermammetric data at 0.8 V(SHE). We believe that the predominant degradation mechanism at this high potential (low oxygen reduction overpotential) is the anodic dissolution of platinum from the oxygen cathode, at least for the constant temperature measurements. It is known that the equilibrium dissolution potential E_{Pt} for nanoparticulate platinum is lower than that for bulk platinum because of the effect of particle curvature on the interfacial energy [36]. In addition, the anodic dissolution of nanoparticulate platinum is believed to occur directly, rather than via a platinum oxide although the latter is thought to occur for bulk platinum [32]. As a result, at 0.8 V(SHE) the Pt/C cathode can be expected to lose platinum by dissolution, resulting in the increase in degradation rate observed when compared with that measured at lower potentials. We expect such a mechanism to be temperature dependent, and so it can be rationalised that the constant temperature cathode, held at a constant 80 °C, experiences a far greater rate of anodic dissolution than the thermammetric sample which has been subject to cyclic temperatures. Although anodic dissolution must also occur from the thermammetrically treated sample, the rate is expected to increase with increase of the applied temperature and so dissolution of Pt would here account for a smaller fraction of the performance loss. The thermammetry sample is, however, subject to thermal cycling leading to particle detachment by thermal fatigue, which is proposed as the major route of performance loss for the thermammetric system. Therefore, it appears that the rate of the simultaneous particle detachment and anodic dissolution at 0.8 V(SHE) and 20 mK s^{-1} is similar to the sole anodic dissolution rate at a constant 80 °C. Since the rate of thermal fatigue is a function of the temperature sweep rate, the approximate coincidence of the two sets of data at 0.8 V(SHE) is fortuitous. This results in the similar extent of degradation with time observed under these conditions.

We also note the following, which is important. It is shown in Fig. 4(a) that the rate of degradation in performance under temperature cycling is initially the same (for the first 2 cycles, both at 20 mK s^{-1}) for the potentials of 0.8 V(SHE) and 0.9 V(SHE), implying that the rate of anodic dissolution of Pt is a small fraction of the total rate of degradation at this stage. We rationalize that the particles that become detached by thermal fatigue in the initial stages must in fact be those that are most easily detached, *i.e.* those that are most loosely bound to the carbon component in the first place, and these therefore detach under few cycles. It must be expected that the bonding between the platinum and the carbon components would show some sort of distribution of strength. As temperature cycling is continued however, and these loosely bound particles are lost, the remaining thermal fatigue rate is slower, because the remaining particles are more tightly bound. At this stage (after cycle 2 in Fig. 4(a)), the rate of degradation of the temperature-cycled samples at 0.8 V(SHE) slows more quickly that the rate at 0.9 V(SHE), and the high-potential degradation rate becomes potential-dependent. In must now be the case, that the rate of anodic dissolution becomes a significant part of the total degradation rate.

There is however, more to the problem than that simple explanation. Fig. 4(a) shows that the rate of decay of the cathodic current density at 0.9 V(SHE) is dependent on the temperature sweep rate throughout the entire time span of the figure, and so the thermal fatigue mechanism must be an important component throughout the decay curve. Thus lowering the potential from 0.9 to 0.8 V(SHE) should not reduce the rate of decay significantly: the graph shows however, that the rate of decay at 0.8 V(SHE) is significantly lower than that at 0.9 V(SHE) after the first 2 temperature cycles. One must therefore be drawn inevitably to the conclusion that the process of anodic dissolution of Pt itself affects the rate of thermal fatigue. We view this as a follows. Although little is known about what links the Pt nanoparticles to the larger carbon nanoparticles, there must be some connecting ligament of platinum which holds the two together. Under anodic dissolution, the binding Pt ligament must also dissolve anodically, and thereby become thinned. Thermal fatigue would therefore be expected to take place more readily and more rapidly on the thinned ligament, than on the same ligament in the absence of anodic dissolution. A faster rate of anodic dissolution of platinum would thereby raise the rate of thermal fatigue, implying that the total degradation rate at high potential would be faster than the sum of the dissolution rate and the potential-independent thermal fatigue rate. It is therefore proposed that anodic dissolution of Pt from the cathode (which is potential-dependent) raises the rate of thermal fatigue (which is otherwise expected to be potential-independent). For the time being, we see no reason to propose the converse mechanism, where the fatigue process may enhance the rate of anodic dissolution of platinum, although this form of coupling between the mechanical and electrochemical processes cannot be ruled out.

These degradation mechanisms may not emulate exactly those in the true PEMFC because of the use here of sulfuric acid electrolyte. Although clearly observable in the aqueous electrolyte system, the mechanisms discussed would still be expected to occur in the PEMFC, but would be expected to be slower because of the solid-state nature of the polymer electrolyte. We seek to extend these investigations to the true PEMFC at a later date.

5. Conclusions

1. A novel electrochemical system is presented which allows determination of the temperature dependence of an electrochemical fuel cell through use of cyclic thermammetry. An informative technique, cyclic thermammetry measurements of the oxygen reduction reaction on a Pt/C cathode in 3 M H_2SO_4 between

25 and 80 °C reveal two simultaneously operating degradation mechanisms that are identified to operate at high cathode potentials of 0.8 V(SHE) and above.
2. One mechanism of degradation is enhanced by thermal cycling and occurs at all electrode potentials. This mechanism involves thermal fatigue at the Pt/C interface causing physical and electrical detachment between the platinum and carbon nanoparticles. Separation of these nanoparticles causes loss of electrocatalytically active surface area from the cathode. To our knowledge, this is the first report of a degradation mechanism activated by temperature cycling for the oxygen reduction cathode and the first report of thermal fatigue at the Pt/C interface.
3. The second mechanism, which occurs only at higher electrode potentials, is the anodic dissolution of the platinum nanoparticles. The rate of anodic dissolution of Pt increases with increase in temperature, but is not accelerated by thermal cycling.
4. At electrode potentials where both mechanisms of degradation operate simultaneously, the anodic dissolution of Pt accelerates the rate of thermal fatigue by weakening the link between the Pt and the carbon nanoparticles.
5. The results verify that two degradation mechanisms operate in tandem at the high cathode potentials expected in operating PEM fuel cells. Revealed using cyclic thermammetry, this technique provides a useful accelerated testing regime for the future development of durable ORR electrocatalysts.

Acknowledgements

We wish to acknowledge the EPSRC for the provision of a studentship (GS). We also thank Johnson–Matthey for financial support and Drs J. Sharman and E. Wright for particularly fruitful discussions.

References

[1] F. de Bruijn, Green Chem. 7 (2005) 132–150.
[2] L. Carrette, K.A. Friedrich, U. Stimming, Chem. Phys. 1 (2000) 162–193.
[3] P. Costamagna, S. Srinivasan, J. Power Sources 102 (2001) 253–269.
[4] M.S. Wilson, F.H. Garzon, K.E. Sickafus, S. Gottesfeld, J. Electrochem. Soc. 140 (1993) 2872–2877.
[5] Z. Wang, P. Zuo, X. Wang, J. Lou, B. Yang, G. Yin, J. Power Sources 184 (2008) 245–250.
[6] X. Yu, S. Ye, J. Power Sources 172 (2007) 145–154.
[7] A. Honji, T. Mori, K. Tamura, Y. Hishinuma, J. Electrochem. Soc. 135 (1988) 355–359.
[8] P.J. Ferreira, G.J.O. la, Y. Shao-Horn, D. Morgan, R. Makharia, S. Kocha, H.A. Gasteiger, J. Electrochem. Soc. 152 (2005) A2256–A2271.
[9] S. Maass, F. Finsterwalder, G. Frank, R. Hartmann, C. Merten, J. Power Sources 176 (2008) 444–451.
[10] R. Borup, J. Meyers, B. Pivovar, Y.S. Kim, R. Mukundan, N. Garland, D. Myers, M. Wilson, F. Garzon, D. Wood, P. Zelenay, K. More, K. Stroh, T. Zawodzinski, J. Boncella, J.E. McGrath, M. Inaba, K. Miyatake, M. Hori, K. Ota, Z. Ogumi, S. Miyata, A. Nishikata, Z. Siroma, Y. Uchimoto, K. Yasuda, K. Kimijima, N. Iwashita, Chem. Rev. 107 (2007) 3904–3951.
[11] M. Umeda, T. Maruta, M. Inoue, A. Nakazawa, J. Phys. Chem. C. 112 (2008) 18098–18103.
[12] K. Yasuda, A. Taniguchi, T. Akita, T. Ioroi, Z. Siroma, Phys. Chem. CH PH 8 (2006) 746–752.
[13] C. Wang, Chem. Rev. 104 (2004) 4727–4766.
[14] H. Ju, H. Meng, C. Wang, Int. J. Heat Mass Trans. 48 (2005) 1303–1315.
[15] C. Song, Y. Tang, J. Zhang, H. Wang, J. Shen, S. McDermid, J. Li, P. Kozak, Electrochim. Acta 52 (2007) 2552–2561.
[16] H. Xu, Y. Song, H.R. Kunz, J.M. Fenton, J. Electrochem. Soc. 152 (2005) A1828–A1836.
[17] N.R. Elezovic, B.M. Babic, N.V.S. Krstajic, L.J. Gojkovic, L.M. Vracar, J. Serb. Chem. Soc. 73 (2008) 641–654.
[18] A. Parthasarathy, S. Srinivasan, A.J. Appleby, C.R. Martin, J. Electrochem. Soc. 139 (1992) 2530–2537.
[19] W. Bi, T.F. Fuller, J. Electrochem. Soc. 155 (2008) B215–B221.
[20] A. R. Kucernak, G. T. Burstein, Unpublished results, 1994.
[21] J.J. Moloney, G.T. Burstein, Extended abstracts of the 203rd Electrochemical Society Meeting, vol. 95, Paris, 2003.
[22] G.T. Burstein, J.J. Moloney, Electrochem. Commun. 6 (2004) 1037–1041.
[23] G.T. Burstein, B.T. Daymond, Corros. Sci. 51 (2009) 2249–2252.
[24] G.T. Burstein, M. Carboneras, B.T. Daymond, Electrochim. Acta 55 (2010) 7860–7866.
[25] R.W. Lindstrom, K. Kortsdottir, M. Wesselmark, A. Oyarce, C. Lagergren, G. Lindbergh, J. Electrochem. Soc. 157 (2010) B1795–B1901.
[26] M. Ciureanu, H. Wang, J. Electrochem. Soc. 146 (1999) 4031–4040.
[27] D.A.J. Rand, R. Woods, J. Electroanal. Chem. 35 (1972) 209–218.
[28] V. Komanicky, K.C. Chang, A. Menzel, N.M. Markovic, H. You, X. Wang, D. Myers, Stability, J. Electrochem. Soc. 153 (2006) B446–B451.
[29] R.M. Darling, J.P. Meyers, J. Electrochem. Soc. 150 (2003) A1523–A1527.
[30] R.M. Darling, J.P. Meyers, J. Electrochem. Soc. 152 (2005) A242–A247.
[31] M. Pourbaix, Atlas of Electrochemical Equilibria in Aqueous Solutions, Pergamon Press, London, 1966.
[32] L. Tang, B. Han, K. Persson, C. Friesen, T. He, K. Sieradzki, G. Ceder, J. Am. Chem. Soc. 132 (2010) 596–600.
[33] D.R. Lide (Ed.), CRC Handbook of Chemistry and Physics, 74th ed., CRC press, Cleveland, 1993.
[34] J.H. Kang, L.D. Menard, R.G. Nuzzo, A.I. Frenkel, J. Am. Chem. Soc. 128 (2006) 12068–12069.
[35] V.I.A. Nikolaev, M. Shipilin, Phys. Solid State 42 (2000) 112–113.
[36] R.S. Goeke, A.K. Datye, P. Atanassov, J. St Pierre, in: The Electrochemical Society, vol. 25, Pennington, ECS Trans. (2009) 593–600.